Heat Transfer Augmentation in an Inclined Lid-Driven Triangular Enclosure Utilizing Nanofluids in Forced Convection Flows

Md. Masum Billah [1,*], Muhammad Sajjad Hossain[1],
Md. Mustafizur Rahman[2] and Abdur Rashid[3]

[1]*Department of Arts and Sciences, Ahsanullah University of Science and Technology, Dhaka-1208, Bangladesh*

[2]*Department of Mathematics, Bangladesh University of Engineering and Technology, Dhaka-1000, Bangladesh*

[3]*Department of Mathematics, Jahangirnagar University, Savar, Dhaka, Bangladesh*

ABSTRACT

Heat transfer enhancement in a two-dimensional inclined lid-driven triangular enclosure utilizing cu-water nanofluids is investigated for various relevant parameters. A model is developed to analyze heat transfer performance of nanofluids inside an enclosure taking into account the force convection parameter, namely Reynolds number, *Re*. The transport equations are solved numerically using the Galerkin finite element method. Comparisons with previously published work on the basis of special cases are performed and found to be in excellent agreement. Results are obtained for a wide range of parameters such as the Richardson number, *Ri*, and Reynolds number, *Re*. Copper-water nanofluids are used with Prandtl number, Pr = 6.2 and Reynolds number, *Re* is varied from 100 to 500. The streamlines, isotherm plots and the variation of the average Nusselt number at the hot surface as well as average fluid temperature in the enclosure are offered and discussed in detailed. It is observed that the force convection parameter strongly influenced the fluid flow and heat transfer in the enclosure at the considered three convective regimes. Furthermore, the variation of the average Nusselt number at the heated surface is found to increase when *Re* increases and average fluid temperature in the cavity decreases with the raise of *Re*.

Keywords: Nanofluids; Triangular enclosure; Finite element method; Solid volume fraction.

*Corresponding author: mmb.as@aust.edu, mmb.edu@gmail.com

1. Introduction

Nanotechnology is considered by many to be one of the significant forces that drive the next major industrial revolution of the present century. It represents the most relevant technological cutting edge currently being explored. It aims at manipulating the structure of the matter at the molecular level with the goal for innovation in virtually every industry and public endeavor including biological sciences, physical sciences, the environment and national security.

Numerous studies on nanofluids are being conducted by talented and studious thermal scientists and engineers all over the world, and they have made scientific breakthroughs not only in discovering unpredicted thermal properties of nanofluids, but also in proposing new mechanisms behind the enhanced thermal properties of nanofluids and thus identifying unusual opportunities to develop them as next generation coolants for computers and safe coolants for nuclear reactors. Various cooling applications of nanofluids include Silicon Mirror Cooling, electronics cooling, vehicle cooling, transformer cooling and so on. Nanofluid technology can help to develop better oils and lubricants. Nanofluids are now being developed for medical applications, including cancer therapy and safer surgery by cooling.

An enormous amount of research interest has been sparked intheir prospective applications of practical problems [1-3]. Phenomena of natural convection in a triangular enclosure are conducted in the literature [4-8]. Chen and Cheng [9] numerically investigated the effects of lid oscillation on the periodic flow pattern and convection heat transfer in a triangular cavity. Natural convection heat transfer in a triangular enclosure with flush mounted heater on the wall [10] and the protruding heaters [11] have been examined. Koca et al. [12] examined the effect of Prandtl number on natural convection heat transfer and fluid flow in triangular enclosures with localized heating. Basak et al. [13] investigated the effects of uniform and non-uniform heating of inclined walls on natural convection flows within an isosceles triangular enclosure using a penalty finite element method with bi-quadratic elements.

The fluids that usually have been used for heat transfer applications, namely water, mineral oils and ethylene glycol have a rather low thermal conductivity and do not meet the rising demand as an efficient heat transfer agent. In order to make up for the growing demands of modern technology, it is very important to develop new types of fluids that will be more effective in terms of heat exchange performance. Such new types of fluids are nanofluids, which are new sort of heat transfer fluids containing a small quantity of nanosized particles that are uniformly and stably suspended in a liquid. It is worth noting that these nanofluids coming have a very high thermal conductivity which can meet the intensifying demand as an efficient heat transfer agent. Numerous researchers have started showing interest in the study of heat transfer characteristics of these nanofluids in recent years. But a clear illustration about the heat transfer through these nanofluids is yet to emerge.

The convective heat transfer feature of nanofluids is influenced by the thermo-physical properties of the base fluid and nano particles. Khanafer et al. [14] made a numerical model to find out natural convection heat transfer in nanofluids. They studied the effect of suspended nanoparticles on the buoyancy-driven heat transfer process and found that in any given Grashof number, heat transfer in the enclosure increased with the volumetric fraction of the copper nanoparticles in water. Jou and Tzeng [15] investigated the heat transfer enhancement utilizing nanofluids in a two-dimensional enclosure

for different relevant parameters. Tiwari and Das [16] studied numerically the heat transfer augmentation in a lid-driven square cavity filled with nanofluids. The authors observed that both the Richardson number and the direction of the moving walls affect the fluid flow and heat transfer in the cavity. A numerical model was presented to analyze the transport mechanism of mixed convection in a lid-driven enclosure packed with nanofluids by Muthtamilselvan et al. [17]. Ghasemi and Aminossadati [18] examined mixed convection heat transfer in a lid-driven triangular enclosure filled with a water–Al_2O_3 nanofluid. The authors showed that the addition of Al_2O_3 nanoparticles enhances the heat transfer rate for different values of Richardson number and for each direction of the sliding wall motion. A parametric study on mixed convection flow in a lid-driven inclined square enclosure filled with water-Al_2O_3 nanofluid was performed by Nada and Chamkha [19]. Mansour et al. [20] performed a numerical simulation on mixed convection flow in a square lid-driven cavity partially heated from below using nanofluid. Eastman et al. [21] conducted pure copper nanoparticles size of less than 10 nm and achieved 40% increase in thermal conductivity for only 0.3% volume fraction of the solid dispersed in ethylene glycol. The particle size effect and potential of nanofluids with smaller particles are presented in their results. Corcione [22] analyzed theoretically the heat transfer features of buoyancy-driven nanofluids inside rectangular enclosures differentially heated at the vertical walls. An experimental investigation of flow and heat transfer characteristics for copper-water based nanofluids through a straight tube with a constant heat flux at the wall was studied by Xuan and Li [23]. Their results demonstrate that the nanofluids give substantial enhancement of heat transfer rate compared to pure water. Talebi et al. [24] numerically studied mixed convection flows in a square lid-driven cavity utilizing nanofluid. Tzeng et al. [25] investigated the effect of nanofluids when used as engine coolants. CuO and Al_2O_3 and antifoam were individually mixed with automatic transmission oil.

Karim et al. [26] examined the unsteady mixed convection heat transfer characteristics of an Ag–water nanofluid confined within a lid-driven square cavity. The authors concluded that the heat transfer rate enhanced to 90% from the heated surface due to increase of Grashof number (Gr) from 10^5 to 10^7 at sinusoidal frequency N =1 and $\tau = 1$.

To investigate the potential of Al_2O_3-water nanofluid, a volume of fluid (VOF) model has been studied to improve the productivity of a single slope solar still by Rashid et al. [27]. The results indicated that the solar still productivity increases with an increase in the solid volume nanoparticles fraction. Since the solid volume fraction increases in the range of 0%–5% then the productivity increases about 25%. Rahman et al. [28] examined the impacts of carbon nano tube (CNT)–water nanofluids in a square enclosure with non-isothermal heating for superior Rayleigh numbers. Alam [29] made a numerical study on natural convective heat transfer of Cobalt-kerosene nanofluid inside a quarter-circular enclosure with uniform and non-uniform heated bottom wall. Weheibi et al [30] conducted a numerical simulation on natural convection heat transfer in a trapezoidal enclosure filled with nanoparticles. Uddin et al. [31] used Nonhomogeneous Dynamic Model to analyze the natural convective heat transfer in homocentric annuli containing nanofluids with oriented magnetic field. Billah et al. [32] studied heat transfer enhancement of copper-water nanofluids in an inclined lid-driven triangular enclosure. Billah et al. [33] examined numerically the heat transfer

enhancement of nanofluids in a lid-driven triangular enclosure having a discrete heater. Later on, Billah et. al. [34] performed a numerical study on unsteady buoyancy-driven heat transfer enhancement of nanofluids in an inclined triangular enclosure.

Due to the rapid development of computer and computational techniques, finite element methods have provided an alternative in dealing with the mixed convection heat transfer in enclosures using nanofluids. To the best knowledge of the authors, little attention has been paid to investigate the heat transfer characteristics of the nanofluids contained in an inclined lid-driven triangular enclosure in forced convection flows. Hence, in this paper the effects of forced convection parameter, Reynolds Number, *Re* in an inclined lid-driven triangular enclosure filled with Cu-water nanofluid is investigated numerically.

2. Mathematical Model

The physical model under current study with the system of coordinates is sketched in Fig. 1. The problem deals with a steady two-dimensional flow of nanofluid contained in an inclined lid-driven triangular enclosure. The length of the base wall and height of the sliding wall of the enclosure are denoted by *L* and *H*, respectively. In addition, the sliding wall of the cavity is kept adiabatic and allowed to move from bottom to top at a constant speed V_0. Moreover, it is assumed that the temperature (T_h) of the bottom wall is higher than the temperature (T_c) of the right inclined wall. The free space in the enclosure is filled with copper water nanofluids. The nanofluid in the enclosure is Newtonian, incompressible and laminar. The nanoparticles are assumed to have uniform shape and size. It is considered that thermal equilibrium exists between the base fluid and nanoparticles, and no slip occurs between the two media.

The thermo-physical properties [23] of the nanofluid are listed in Table 1. The physical properties of the nanofluid are considered to be constant except the density variation in the body force term of the momentum equation which is satisfied by the Boussinesq's approximation. Under the above assumptions, the system of equations governing the two-dimensional motion of a nanofluid is as follows:

$$\frac{\partial u}{\partial x} + \frac{\partial v}{\partial y} = 0 \tag{1}$$

$$u\frac{\partial u}{\partial x} + v\frac{\partial u}{\partial y} = -\frac{1}{\rho_{nf}}\frac{\partial p}{\partial x}$$
$$+\frac{\mu_{nf}}{\rho_{nf}}\left(\frac{\partial^2 u}{\partial x^2} + \frac{\partial^2 u}{\partial y^2}\right) \tag{2}$$
$$+\frac{(\rho\beta)_{nf}}{\rho_{nf}}(T-T_c)g\sin\phi$$

$$u\frac{\partial v}{\partial x} + v\frac{\partial v}{\partial y} = -\frac{1}{\rho_{nf}}\frac{\partial p}{\partial y}$$
$$+\frac{\mu_{nf}}{\rho_{nf}}\left(\frac{\partial^2 v}{\partial x^2} + \frac{\partial^2 v}{\partial y^2}\right)+ \tag{3}$$
$$\frac{(\rho\beta)_{nf}}{\rho_{nf}}(T-T_c)g\cos\phi$$

$$u\frac{\partial T}{\partial x} + v\frac{\partial T}{\partial y} = \alpha_{nf}\left(\frac{\partial^2 T}{\partial x^2} + \frac{\partial^2 T}{\partial y^2}\right) \tag{4}$$

The effective density ρ_{nf} of the nanofluid is defined by

$$\rho_{nf} = (1-\delta)\rho_f + \delta\rho_s \tag{5}$$

where δ is the solid volume fraction of nanoparticles.
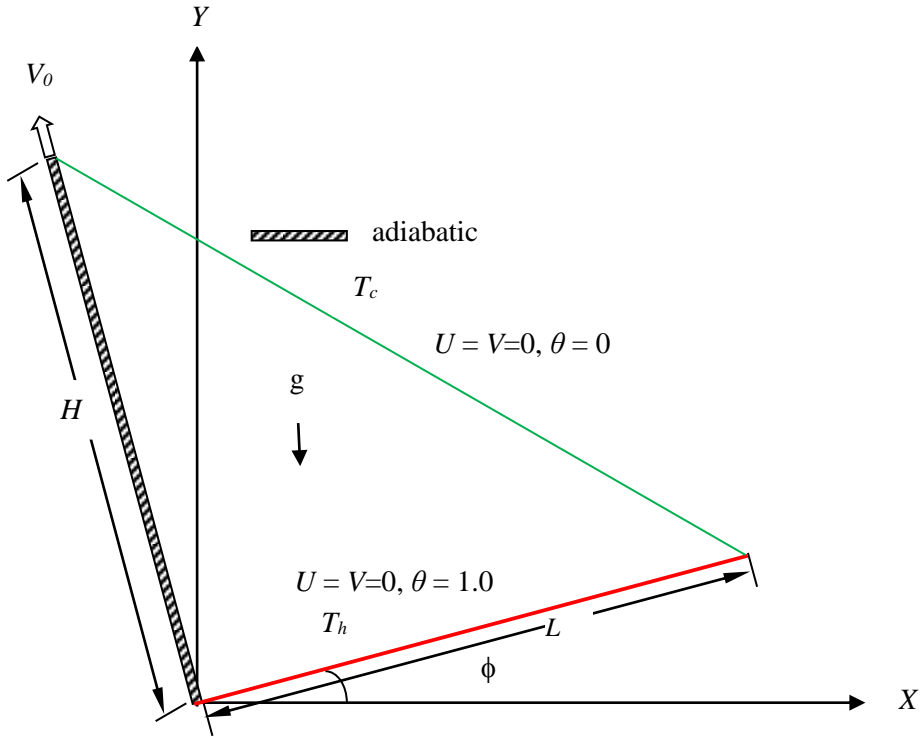
4

Fig. 1. Schematic of the problem with the domain and boundary conditions.

In addition, the thermal diffusivity α_{nf} of the nanofluid can be expressed as:

$$\alpha_{nf} = \frac{k_{nf}}{\left(\rho c_p\right)_{nf}} \qquad (6)$$

The heat capacitance of nanofluids can be defined as:

$$\left(\rho c_p\right)_{nf} = (1-\delta)\left(\rho c_p\right)_f + \delta\left(\rho c_p\right)_s \qquad (7)$$

In addition, $\left(\rho\beta\right)_{nf}$ is the thermal expansion coefficient of the nanofluid and it can be determined by

$$\left(\rho\beta\right)_{nf} = (1-\delta)(\rho\beta)_f + \delta(\rho\beta)_s \qquad (8)$$

Moreover, μ_{nf} is the dynamic viscosity of the nanofluid introduced by Brikman [30] as

$$\mu_{nf} = \frac{\mu_f}{(1-\delta)^{2.5}} \qquad (9)$$

The effective thermal conductivity of nanofluid was intoduced by Kanafer et al. [14] as:

$$\frac{k_{nf}}{k_f} = \frac{k_s + 2k_f - 2\delta\left(k_f - k_s\right)}{k_s + 2k_f + \delta\left(k_f - k_s\right)} \qquad (10)$$

where k_s is the thermal conductivity of the nanoparticles and k_f is the thermal conductivity of base fluid.

Introducing the following dimensionless variables

$$X = \frac{x}{L},\, Y = \frac{y}{L},\, U = \frac{u}{V_0},$$

$$V = \frac{v}{V_0},\, P = \frac{\left(p + \rho gy\right)L^2}{\rho_{nf}\, V_0^{\,2}}, \qquad (11)$$

$$\theta = \frac{\left(T - T_c\right)}{\left(T_h - T_c\right)}$$

the governing equations may be written in the dimensionless form as

$$\frac{\partial U}{\partial X} + \frac{\partial V}{\partial Y} = 0 \qquad (12)$$

5

$$U\frac{\partial U}{\partial X} + V\frac{\partial U}{\partial Y} = -\frac{\partial P}{\partial X}$$

$$+\frac{1}{Re}\frac{\rho_f}{\rho_{nf}}\frac{1}{(1-\delta)^{2.5}}\left(\frac{\partial^2 U}{\partial X^2}+\frac{\partial^2 U}{\partial Y^2}\right) \qquad (13)$$

$$+\frac{(\rho\beta)_{nf}}{\rho_{nf}\beta_f}Ri\,\theta\sin\phi$$

$$U\frac{\partial V}{\partial X} + V\frac{\partial V}{\partial Y} = -\frac{\partial P}{\partial Y}$$

$$+\frac{1}{Re}\frac{\rho_f}{\rho_{nf}}\frac{1}{(1-\delta)^{2.5}}\left(\frac{\partial^2 V}{\partial X^2}+\frac{\partial^2 V}{\partial Y^2}\right) \qquad (14)$$

$$+\frac{(\rho\beta)_{nf}}{\rho_{nf}\beta_f}Ri\,\theta\cos\phi$$

$$U\frac{\partial\theta}{\partial X} + V\frac{\partial\theta}{\partial Y} = \frac{\alpha_{nf}}{\alpha_f}\frac{1}{Re\,Pr}$$

$$\left(\frac{\partial^2\theta}{\partial X^2}+\frac{\partial^2\theta}{\partial Y^2}\right) \qquad (15)$$

The nondimensional numbers that appear in equations (13)-(15) are as follows: Reynolds number $Re = V_0 L/\upsilon_f$, Prandtl number $Pr = \nu_f/\alpha_f$ and Richardson number $Ri = Gr/\mathrm{Re}^2$, where $Gr = g\beta_f(T_h - T_c)L^3/\nu_f^2$ is the Grashof number and $\mathrm{Re} = V_0 L/\nu_f$ is the Reynolds number.

The appropriate boundary conditions for the governing equations are

on the bottom wall: $U = V = 0$, $\theta = 1$

on the left inclined wall: $U = 0, V = 1, \frac{\partial\theta}{\partial N} = 0$

on the right inclined wall: $U = V = 0$, $\theta = 0$

where N is the non-dimensional distances either X or Y direction acting normal to the surface.

The average Nusselt number at the heated surface of the cavity may be expressed as

$$Nu_{av} = -\frac{k_{nf}}{k_f}\int_0^1\frac{\partial\theta}{\partial Y}dX \qquad (16)$$

and average fluid temperature in the enclosure may be defined as
$$\theta_{av} = \int\theta\,d\overline{V}\,/\overline{V} \qquad (17)$$

Table 1. Thermophysical properties of water and copper [23].

Property	water	Copper
c_p	4179	385
P	997.1	8933
K	0.613	401
B	2.1×10^{-4}	1.67×10^{-5}

The fluid motion is displayed using the stream function ψ obtained from velocity components U and V. The relationships between stream function and velocity components for two dimensional flows can be expressed as:

$$U = \frac{\partial\psi}{\partial Y}, \; V = -\frac{\partial\psi}{\partial X} \qquad (18)$$

3. Solution Procedure

3.1 Numerical Scheme

The Galerkin finite element method is used to solve the non-dimensional governing equations along with boundary conditions. The advantages of the finite element method (FEM) are its ability to deal with the complex 2D or 3D domains and it has higher accuracy and rapid convergence. Another benefit of it is that of the specific mode to deduce the equations for each element which are then assembled. Therefore, the addition of new elements by refinement of the existing ones is not a major problem. The computational domains

with irregular geometries by a collection of finite elements make the method a valuable practical tool for the solution of the boundary value problems arising in various fields of engineering. For the other methods, the mesh refinement is a major task and could involve the rewriting of the program. But for all the methods used for the discrete analogue of the initial equations, the obtained system of simultaneous equations must be solved. That is why, the present work emphasizes the use of FEM to solve flow and heat transfer problems.The equation of continuity has been used as a constraint due to mass conservation and this restriction may be used to find the pressure distribution. Penalty finite element method [28] is used to solve Eqs. (13) - (15), where the pressure P is eliminated by a penalty constraint γ and the incompressibility criteria given by Eq. (12) results in

$$P = -\gamma \left(\frac{\partial U}{\partial X} + \frac{\partial V}{\partial Y} \right) \qquad (19)$$

The continuity equation is automatically

fulfilled for large values of γ.

The momentum equations reduce to

$$U \frac{\partial U}{\partial X} + V \frac{\partial U}{\partial Y} = \gamma \frac{\partial}{\partial X} \left(\frac{\partial U}{\partial X} + \frac{\partial V}{\partial Y} \right)$$

$$+ \frac{1}{Re} \frac{\rho_f}{\rho_{nf}} \frac{1}{(1-\delta)^{2.5}} \left(\frac{\partial^2 U}{\partial X^2} + \frac{\partial^2 U}{\partial Y^2} \right) \qquad (20)$$

$$+ \frac{(\rho\beta)_{nf}}{\rho_{nf}\beta_f} Ri\,\theta \sin\phi$$

$$U \frac{\partial V}{\partial X} + V \frac{\partial V}{\partial Y} = \gamma \frac{\partial}{\partial Y} \left(\frac{\partial U}{\partial X} + \frac{\partial V}{\partial Y} \right)$$

$$+ \frac{1}{Re} \frac{\rho_f}{\rho_{nf}} \frac{1}{(1-\delta)^{2.5}} \left(\frac{\partial^2 V}{\partial X^2} + \frac{\partial^2 V}{\partial Y^2} \right) \qquad (21)$$

$$+ \frac{(\rho\beta)_{nf}}{\rho_{nf}\beta_f} Ri\,\theta \cos\phi$$

Expanding the velocity components (U, V), and temperature (θ) using basis set $\{\Phi_k\}_{k=1}^{N}$ as

$$U \approx \sum_{k=1}^{N} U_k \Phi_k (X,Y),\ V$$

$$\approx \sum_{k=1}^{N} V_k \Phi_k (X,Y), \text{and} \qquad (22)$$

$$\theta \approx \sum_{k=1}^{N} \theta_k \Phi_k (X,Y)$$

Then the Galerkin finite element method yields the subsequent nonlinear residual equations for Eqs. (15), (20) and (21) respectively, at nodes of the internal domain Ω:

$$R_i^{(1)} = \sum_{k=1}^{N} \theta_k \int_{\Omega} \left[\left(\sum_{k=1}^{N} U_k \Phi_k \right) \frac{\partial \Phi_k}{\partial X} + \left(\sum_{k=1}^{N} V_k \Phi_k \right) \frac{\partial \Phi_k}{\partial Y} \right] \Phi_i dXdY$$

$$- \frac{\alpha_{nf}}{\alpha_f\, Re\, Pr} \sum_{k=1}^{N} \theta_k \int_{\Omega} \left[\frac{\partial \Phi_i}{\partial X} \frac{\partial \Phi_k}{\partial X} + \frac{\partial \Phi_i}{\partial Y} \frac{\partial \Phi_k}{\partial Y} \right] dXdY \qquad (23)$$

7

$$R_i^{(2)} = \sum_{k=1}^{N} U_k \int_{\Omega} \left[\left(\sum_{k=1}^{N} U_k \Phi_k \right) \frac{\partial \Phi_k}{\partial X} + \left(\sum_{k=1}^{N} V_k \Phi_k \right) \frac{\partial \Phi_k}{\partial Y} \right]$$

$$\Phi_i dXdY - \gamma \left[\sum_{k=1}^{N} U_k \int_{\Omega} \frac{\partial \Phi_i}{\partial X} \frac{\partial \Phi_k}{\partial X} dXdY \right]$$

$$- \gamma \left[\sum_{k=1}^{N} V_k \int_{\Omega} \frac{\partial \Phi_i}{\partial X} \frac{\partial \Phi_k}{\partial Y} \right] dXdY$$

$$- \frac{1}{Re} \frac{\rho_f}{\rho_{nf}} \frac{1}{\left(1-\delta\right)^{2.5}}$$

$$\sum_{k=1}^{N} U_k \int_{\Omega} \left[\frac{\partial \Phi_i}{\partial X} \frac{\partial \Phi_k}{\partial X} + \frac{\partial \Phi_i}{\partial Y} \frac{\partial \Phi_k}{\partial Y} \right] dXdY$$

$$- \frac{(\rho\beta)_{nf}}{\rho_{nf}\beta_f} Ri \sin\phi$$

$$\int_{\Omega} \left(\sum_{k=1}^{N} \theta_k \Phi_k \right) \Phi_i dXdY \tag{24}$$

$$R_i^{(3)} = \sum_{k=1}^{N} V_k \int_{\Omega} \left[\left(\sum_{k=1}^{N} U_k \Phi_k \right) \frac{\partial \Phi_k}{\partial X} + \left(\sum_{k=1}^{N} V_k \Phi_k \right) \frac{\partial \Phi_k}{\partial Y} \right] \Phi_i dXdY$$

$$- \gamma \left[\sum_{k=1}^{N} U_k \int_{\Omega} \frac{\partial \Phi_i}{\partial X} \frac{\partial \Phi_k}{\partial X} dXdY \right]$$

$$- \gamma \left[\sum_{k=1}^{N} V_k \int_{\Omega} \frac{\partial \Phi_i}{\partial X} \frac{\partial \Phi_k}{\partial Y} \right] dXdY$$

$$- \frac{1}{Re} \frac{\rho_f}{\rho_{nf}} \frac{1}{\left(1-\delta\right)^{2.5}}$$

$$\sum_{k=1}^{N} V_k \int_{\Omega} \left[\frac{\partial \Phi_i}{\partial X} \frac{\partial \Phi_k}{\partial X} + \frac{\partial \Phi_i}{\partial Y} \frac{\partial \Phi_k}{\partial Y} \right] dXdY$$

$$- \frac{(\rho\beta)_{nf}}{\rho_{nf}\beta_f} Ri \cos\phi$$

$$\int_{\Omega} \left(\sum_{k=1}^{N} \theta_k \Phi_k \right) \Phi_i dXdY \tag{25}$$

Three points Gaussian quadrature is used to evaluate the integrals in the residual equations. The non-linear residual equations (Eqs. (23) – (25)) are solved using Newton–Raphson method to determine the coefficients of the expansions in Eq. (22). The convergence of solutions is assumed when the relative error for each variable between consecutive iterations is recorded below the convergence criterion ε such that $\left| \Gamma^{n+1} - \Gamma^n \right| \leq 10^{-4}$, where n is number of iteration and Γ is the general dependent variable.

3.2 Grid independence study

A grid refinement study has been done for $Re = 100$, $Ri = 1$, $\phi = 60$ and $\delta = 0.04$ in an inclined lid-driven triangular enclosure. Five different non-uniform grid systems are examined with the following number of elements within the resolution field: 1486, 2808, 3490, 4894 and 5588. The numerical design is carried out for highly precise key in the average Nusselt number (Nu_{av}) for the aforesaid elements to develop an understanding of the grid fineness as shown in Fig. 2(a). The scale of Nu_{av} for 4894 elements shows a little difference from the results obtained for the other elements. Hence a grid size of 4894 elements is found to meet the requirements of both the grid independency study and the computational time limits.
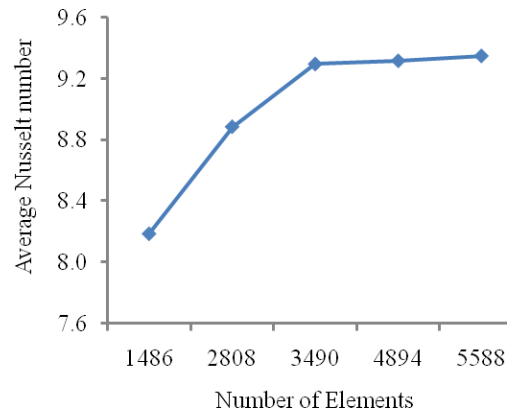

Fig. 2(a). Grid independency study for $Re = 100$, $Ri = 1$, $\phi = 60$ and $\delta = 0.04$.

8

3.3 Code validation

In order to check the accuracy of the numerical technique employed for the solution of the considered problem, the present numerical code was validated with the published work of Yesiloz and Aydin [35]. The physical problem studied by Yesiloz and Aydin [35] was steady laminar natural convection inside a water-filled right triangular enclosure heated from below and cooled from sidewall while the remaining wall, i. e. the hypotenuse was adiabatic.

The comparison of the results obtained by the present numerical code with those of Yesiloz and Aydin [35] with respect to streamlines and isotherms is shown in Fig. 2(b). The computed results are in very good agreement with the Yesiloz and Aydin [35] solution. This validation boosts the confidence in the numerical outcome of the present study.
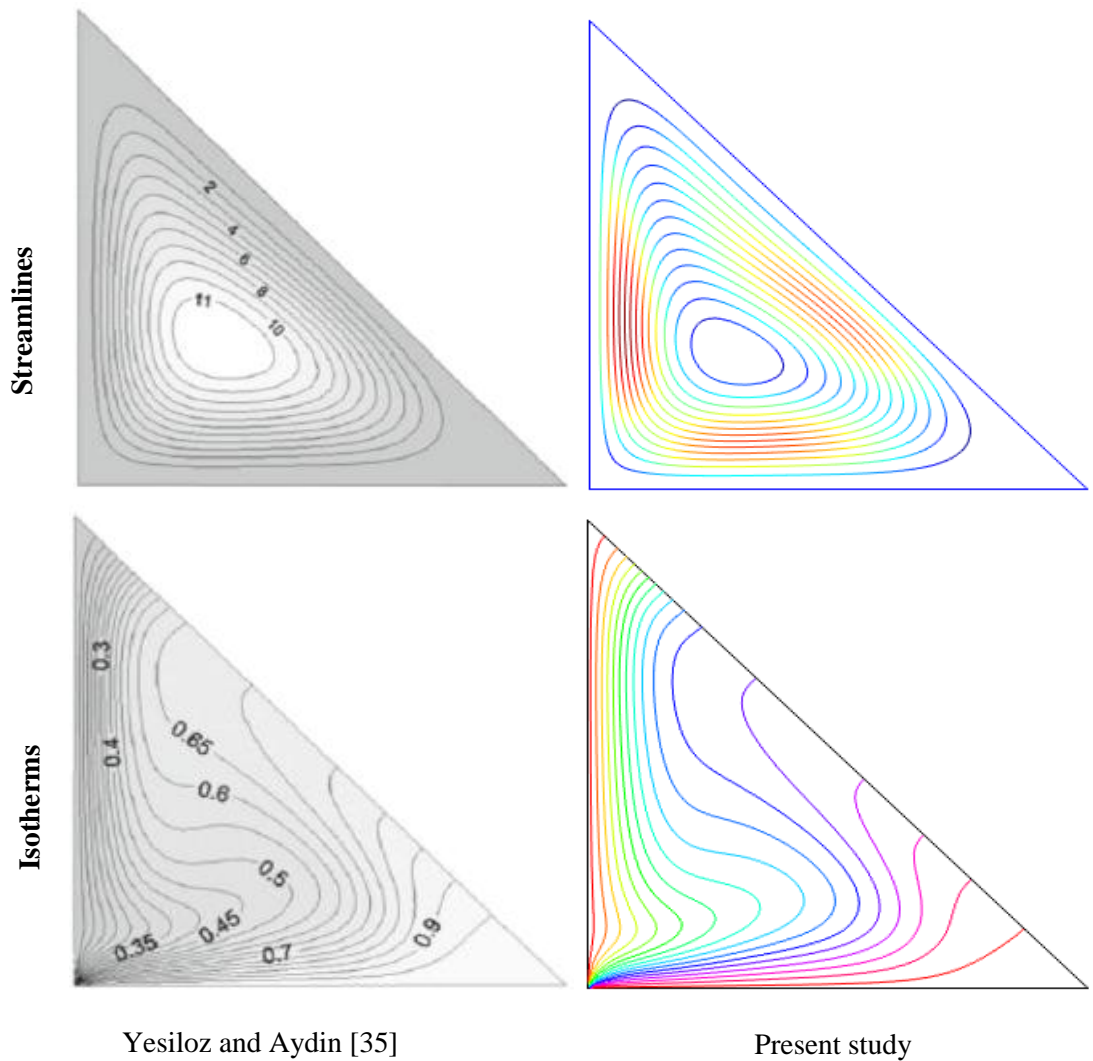

Yesiloz and Aydin [35]   Present study

Fig. 2(b). Comparison of streamlines and isotherms between Yesiloz and Aydin [35] (left) and the present work (right) for $Ra = 10^5$.
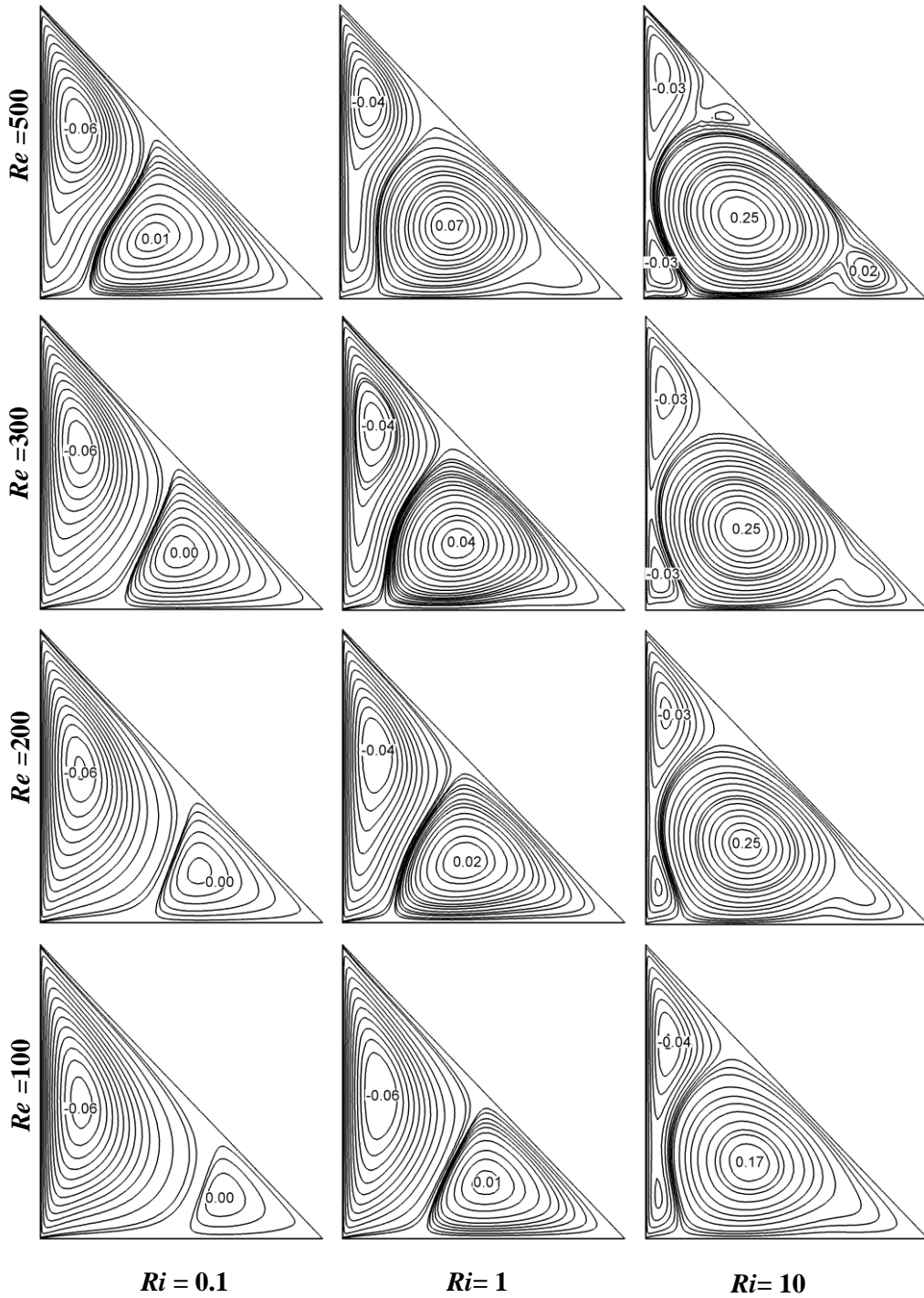
9

Fig. 3. Streamlines for different values of Reynolds number *Re* and Richardson number *Ri*, while $\delta = 0.04$ and $\phi = 60°$.

4. Results and discussion

The present numerical study is carried out for copper-water nanofluids as working fluid with Prandtl number of 6.2. In this analysis, we investigate the effects of Reynolds number (Re), and Richardson number (Ri). Here, the effect of Reynolds number is investigated in the range of 100 to 500, while the δ and tilt angle ϕ are kept fixed at 0.04 and 60, respectively.

It is worth noting that the value of Ri is varied from 0.1 to 10 by changing Grashof number Gr to cover the forced convection dominated region, pure mixed convection and free convection dominated region. Moreover, the results of this study are presented in terms of streamlines and isotherms. Furthermore, the heat transfer effectiveness of the enclosure is displayed in terms of average Nusselt number Nu_{av} and the dimensionless average temperature of the cavity θ_{av}.

4.1 Flow and Thermal Fields

The effect of Reynolds Number Re and Ri on the fluid flow and temperature distribution in the cavity are illustrated in Figs. 3 and 4 by plotting the streamlines and isotherms for Re = 100, 200, 300 and 500 and various Ri (0, 1 and 10), while $\delta = 0.04$ and $\phi = 60^{\circ}$.

The basic flow structure in the absence of natural convection effect is presented in the left bottom corner of Fig. 3 at $Re = 100$. It is seen clearly that for $Ri = 0.1$ and low Reynolds number ($Re = 100$), the forced convection plays a dominant role, and the recirculation flow is mostly generated only by the moving lid.The fluid flow in a two dimensional lid-driven triangular enclosure is characterized by a main circulating cell (major cell) near the vicinity of the sliding left surface in the enclosure developed by the lid and a weaker anticlockwise rotating cell close to the right bottom corner for all values of Re. As can easily be seen from the left column of Fig. 3, the key cell is created by the lid exhausting the neighboring fluid. Though the flow strength of the key cell is identical, the size of the key cell is affected for all values of Re.

Moreover, it is found from the streamlines that the size of the anticlockwise rotating cell is escalating very moderately when Re is increased. With an increment in Re at $Ri = 1$, buoyancy driven vortex becomes stronger than the vortex due to the moving lid. Finally, for $Ri = 10$ and different values of Re (= 100, 200, 300 and 500) the flow patterns are characterized by two asymmetrical vortices that occupy the entire cavity as reflected in the right column of Fig. 3. It seems that the mechanical effect generated by the moving lid is dominated by the buoyancy forces.

The isotherm patterns for different Reynolds number and Richardson number at $\delta = 0.04$ are described in Fig. 4. From the left column of this figure, it is seen that the isotherms for different values of Re at $Ri = 0.1$ are clustered near the heated surface of the enclosure, which indicates a steep temperature gradient along the horizontal direction in this region. Moreover, in the remaining area of the cavity, the temperature gradients are very small due to the mechanically-driven circulations. It is also noticed that the thermal layer near the hot surface becomes moderately thin with increasing Re. Also, at $Ri = 1$ the thermal layer near the hot surface becomes thin and wavy isotherms are observed for higher Re, which indicates the steeper thermal gradient becomes stronger with escalating Re. Furthermore, as Ri increases to 10 the thermal layer near the hot surface become very thin and the thermal spot is developed between the two rotating cells.
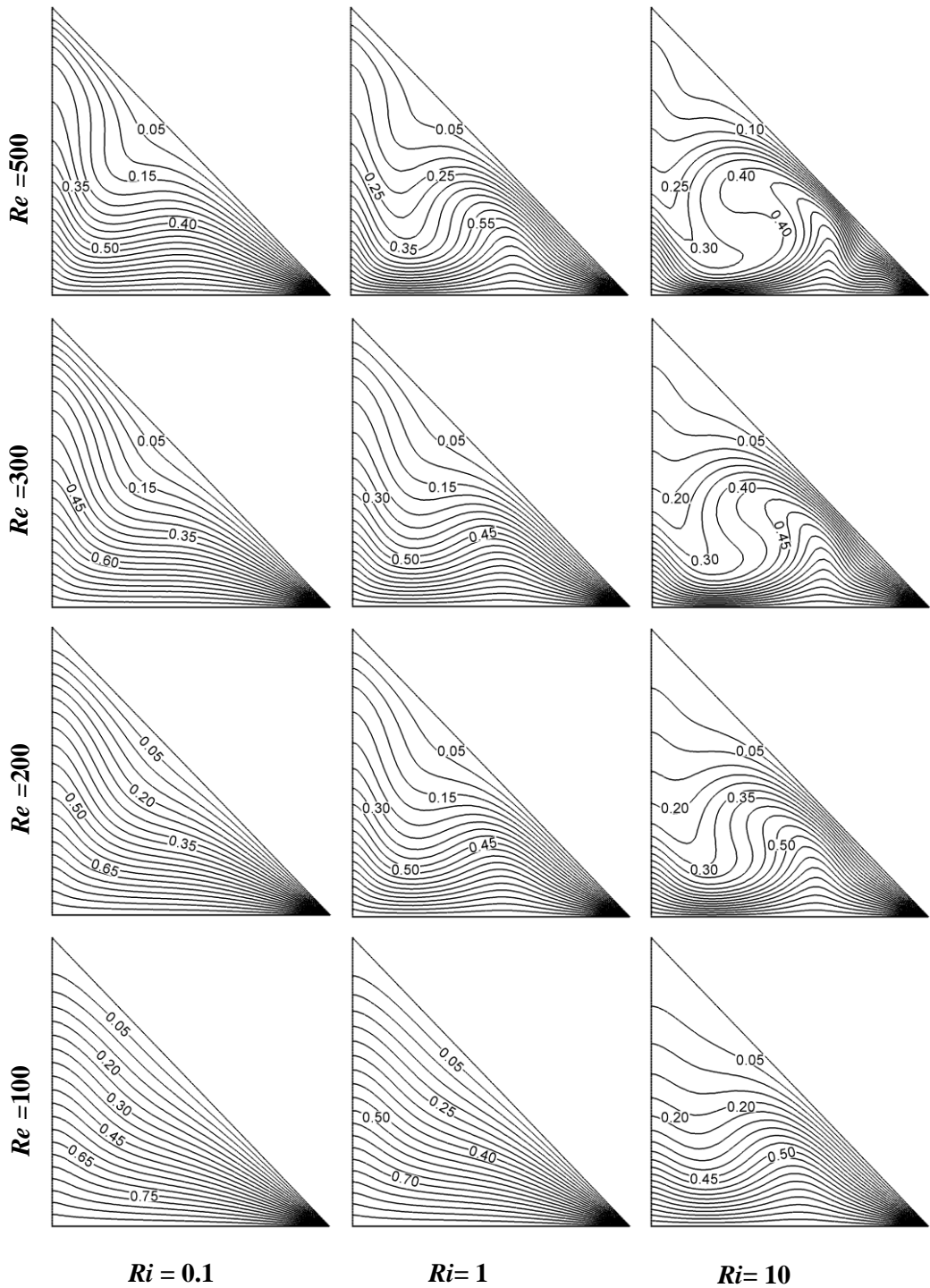
Fig. 4. Isotherms for different values of Reynolds number *Re* and Richardson number *Ri*, while δ = 0.04 and ϕ = 60°.

4.2 Heat Transfer

The average Nusselt number at the heat source is plotted as a function of Richardson number for a particular Reynolds number is as shown in Fig. 5. Fig. 5 presents a very illustrative picture of how the heat is transferred in accordance with *Re* and *Ri*. Keeping *Re* constant, the average Nusselt number at the heated surface increases gradually with increasing value of *Ri*. Also, the average Nusselt number at the heated surface is found to increase as *Re* increases at fixed *Ri*. These results are probable because nanoparticles increase heat absorbing capacity of the base fluid. Therefore, it can be concluded that more heat transfer from the heat source is expected in the case of a large parameter value of *Re* or *Ri*. One can notice that the values of *Nu* are lower for the pure mixed convection (*Ri* = 1), when compared with that for the other values of *Ri*. Nevertheless, the values of Nu_{av} are always maximum for the higher value of *Re* (= 500).
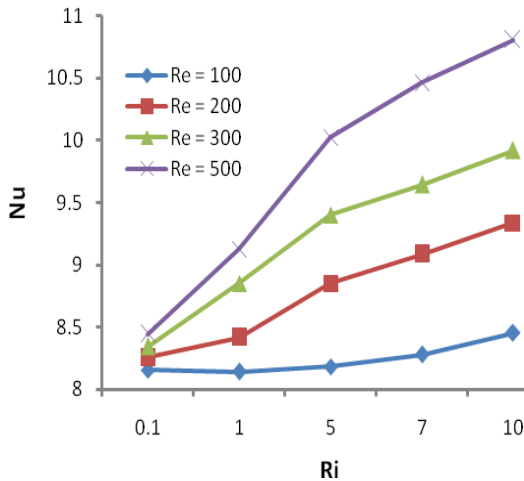

Fig.5. Effect of Reynolds number *Re* on average Nusselt number at the heated surface in the cavity,while $\delta = 0.04$ and $\phi = 60°$.

The effect of Reynolds number *Re* on average fluid temperature θ_{av} in the cavity is revealed in the Fig. 6. From this figure, it

can clearly be seen that the value of θ_{av} decreases promptly with the raise of *Ri* for all considered Reynolds number.
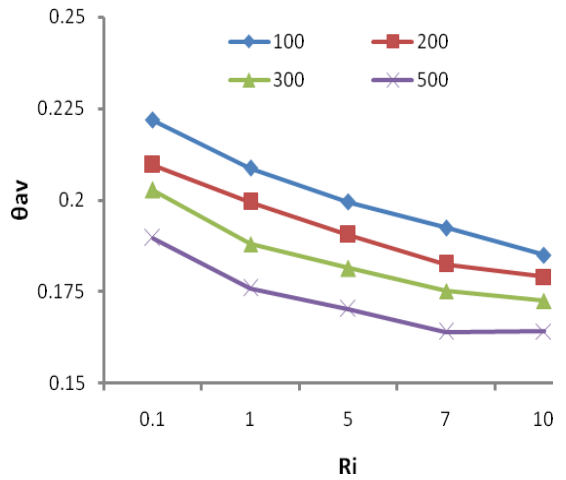

Fig. 6. Effect of Reynolds number *Re* on average fluid temperature in the cavity, while $\delta = 0.04$ and $\phi = 60°$.

5. Conclusion

Mixed convection in a lid-driven inclined triangular enclosure filled with nanofluids is studied numerically. Results for various parametric conditions are presented and discussed. From the above study, the following conclusions are made:

- Forced convection parameter *Re* has a great significant effect on the streamlines and isotherms field. Buoyancy-induced vortex in the streamlines increased and thermal layer near the heated surface become thin and concentrated with increasing *Re*. Besides, the heat transfer increased by nearly 23.45% at *Ri* =1 but it increased by almost 30.83% at *Ri* =10 as *Re*increases from100 to 500.

- The average Nusselt numbers at the heated surface is always upper and the average temperature in the cavity is inferior for the large value of *Re*.

13

- Nanofluids are capable to modify the flow pattern.

Nomenclatures

c_p Specific heat at constant pressure

g gravitational acceleration (ms^{-2})

H enclosure height (m)

k thermal conductivity (Wm^{-1}K^{-1})

L length of the cavity (m)

Nu Nusselt number

p dimensional pressure (Nm^{-2})

P dimensionless pressure

Pr Prandtl number

Re Reynolds number

Ri Richardson number

T temperature (K)

u horizontal velocity component (ms^{-1})

U dimensionless horizontal velocity component

v vertical velocity component (ms^{-1})

V dimensionless vertical velocity component

V_0 lid velocity (ms^{-1})

$\bar{V}$ cavity volume (m^3)

x horizontal coordinate (m)

X dimensionless horizontal coordinate

y vertical coordínate (m)

Y dimensionless vertical coordinate

Greek symbols

α thermal diffusivity (m^{2}s^{-1})

β thermal expansion coefficient (K^{-1})

δ solid volume fraction

μ dynamic viscosity (kg m^{-1}s^{-1})

v kinematic viscosity (m^{2}s^{-1})

θ non-dimensional temperature

ρ density (kg m^{-3})

ψ Streamfunction

ϕ tilt angle, degree (^{0})

γ penalty parameter

Subscripts

av   Average

h   Hot

c   Cold

f   Fluid

nf   Nanofluid

s   Solid nanoparticle

References

[1] Holtzman GA, Hill RW, Bal KS. Laminar natural convection in isosceles triangular enclosures heated from below and symmetrically cooled from above. J Heat TransferTransactions of the ASME 2000; 122 : 485–91.

[2] Haese PM, Teubner MD. Heat exchange in an attic space. IntJ Heat Mass transfer 2002;45(25):4925–36.

[3] Joudi KA, Hussein IA, Farhan AA. Computational model for a prism shaped storage solar collector with a right triangular cross section. Energy Conversion and Management 2004;45: 337–342.

[4] Saha SC, Gu YT. Natural convection in a triangular enclosure heated from below and non-uniformly cooled from top. Int J Heat and Mass Transfer 2015; 80:529-538.

[5] Lei C, Patterson JC. Unsteady natural convection in a triangular enclosure induced by absorption of radiation. JFluid Mechanics 2002; 460:181–209.

[6] Lei C, Patterson JC. Unsteady natural convection in a triangular enclosure induced by surface cooling. Int J Heat Fluid Flow 2005; 26: 307–321

[7] Basak T, Roy S, Thirumalesha Ch. Finite element analysis of natural convection in a triangular enclosure: Effects of various thermal boundary conditions. Chemical Engineering Science 2007; 62:2623–2640.

[8] Omri A, Najjari M, Nasrallah SB. Numerical analysis of natural buoyancy induced regimes in isosceles triangular cavities. Numer Heat Transfer, Part-A Appl. 2007; 52: 661–678.

[9] Chen CL, Cheng CH. Numerical study of the effects of lid oscillation on the periodic flow pattern and convection heat transfer in a triangular cavity. Int Comm Heat Mass Transfer 2009; 36: 590-596

[10] Varol Y, Koca A, Oztop HF. Natural convection in a triangle enclosure with flush mounted heater on the wall. Int

Commun Heat Mass Transfer 2006; 33: 951-958.

[11] Varol Y, Oztop HF, Yilmaz T.Natural convection in triangular enclosures with protruding isothermal heater. Int J Heat Mass Transfer 2007; 50: 2451–2462.

[12] Koca A, Oztop HF, Varol Y. The effects of Prandtl number on natural convection in triangular enclosures with localized heating from below. Int Commun Heat Mass Transfer 2007; 34:511–519.

[13] Basak T, Roy S, Babu SK, Balakrishnan AR. Finite element analysis of natural convection flow in an isosceles triangular enclosure due to uniform and non-uniform heating at the side walls. Int J Heat Mass Transfer 2008;51: 4496-4505.

[14] Khanafer K, Vafai K, Lightstone M. Buoyancy-driven heat transfer enhancement in a two-dimensional enclosure utilizing nanofluids. Int J Heat Mass Transfer 2003; 46:3639-3653.

[15] Jou RY, Tzeng SC. Numerical research of nature convective heat transfer enhancement filled with nanofluids in rectangular enclosures. Int Commun Heat Mass Transfer 2006; 33:727-736.

[16] Tiwari RK, Das MK. Heat transfer augmentation in a two-sided lid-driven differentially heated square cavity utilizing nanofluids. Int J of Heat Mass Transfer 2007; 50: 2002-2018.

[17] Muthtamilselvan M, Kandaswamy P, LeeJ. Heat transfer enhancement of copper-water nanofluids in a lid-driven enclosure. Commun Nonlinear Sci Numer Simulat 2010;15:1501-1510.

[18] Ghasemi B, Aminossadati SM. Mixed convection in a lid-driven triangular enclosure filled with nanofluids. Int Commun Heat Mass Transfer 2010; 37:1142–1148.

[19] Nada EA, Chamkha AJ. Mixed convection flow in a lid-driven inclined square enclosure filled with a nanofluid. European J Mechanics B/Fluids 2010; 29:472-482.

[20] Mansour MA, Mohamed RA, Abd-Elaziz MM, Ahmed SE. Numerical simulation of mixed convection flows in a square lid-driven cavity partially heated from below using nanofluid. Int Commun Heat Mass Transfer 2010; 37:1504–1512.

[21] Eastman JA, Choi SUS, Li S, Yu W, Thompson LJ. Anomalously increased effective thermal conductivities of ethylene glycol-based nanofluids containing copper nanoparticles. Appl Phys Lett 2001; 78:718-20.

[22] Corcione M. Heat transfer features of buoyancy-driven nanofluids inside rectangular enclosures differentially heated at the sidewalls. Int J Thermal Sciences 2010; 49:1536-1546.

[23] Xuan Y, Li Q. Investigation on Convective Heat Transfer and Flow Features of Nanofluids.ASME J Heat Transfer 2003; 125:151-155.

[24] Talebi F, Mahmoudi AH, Shahi M. Numerical study of mixed convection flows in a square lid-driven cavity utilizing nanofluid. Int Commun Heat Mass Transfer 2010; 37:79-90.

[25] Tzeng SC, Lin CW, Huang KD. Heat transfer enhancement of nanofluids in rotary blade coupling of four-wheel-drive vehicles. Acta Mechanica 2005; 179:11-23.

[26] Karim MA, Billah MM, Newton MTT, Rahman MM. Influence of the periodicity of sinusoidal boundary condition on the unsteady mixed convection within a square enclosure using an Ag–water nanofluid. Energies 2017;10(12):1-21.

[27] Rashidi S, Akar S, Bovand M, Ellahi R. Volume of fluid model to simulate the nanofluid flow and entropy generation in a single slope solar still. Renew Eng 2018; 115:400–410.

[28] Rahman MM, Öztop HF, Steele M, Naim AG, Al-Salem K, Ibrahim TA. Unsteady natural convection and statistical analysis in CNT-water filled cavity with non-isothermal heating. Int Communheat mass transfer 2015; 64: 50–60.

[29] Alam MS. Natural convective heat transfer of Cobalt-kerosene nanofluid inside a Quarter-circular enclosure with

uniform and non-uniform heated bottom wall using two-component nonhomogeneous model. Thammasat Int J of Science Technology 2017; 22(1): 45-66.

[30] Al-Weheibi SM, Rahman MM, Alam MS, Vajravelu K. Numerical simulation of natural convection heat transfer in a trapezoidal enclosure filled with nanoparticles. IntJMechanical Sciences 2017;131-132:599-612.

[31] Uddin MJ, Rahman MM, Alam MS. Analysis of natural convective heat transfer in homocentric annuli containing nanofluids with oriented magnetic field using nonhomogeneous dynamic model. Neural Computing & Applications 2018; 30:3189-3208.

[32] Billah MM, Rahman MM, Shahabuddin M, Azad AK. Heat transfer enhancement of copper-water nanofluids in an inclined lid-driven triangular enclosure. J Scientific Research 2011; 3(2): 525-538.

[33] Billah MM, Rahman MM, Sharif UM, Heat transfer enhancement of nanofluids in a lid-driven triangular enclosure having a discrete heater. Procedia Eng 2013;56:330-336.

.

[34] Billah MM, Rahman MM, Razzak MA, Saidur R, Mekhilef S. Unsteady buoyancy-driven heat transfer enhancement of nanofluids in an inclined triangular enclosure. Int Commun. Heat Mass Transfer 2013;49:115-127.

[35] Yesiloz G, Aydin O. Laminar natural convection in right-angled triangular enclosures heated and cooled on adjacent walls. Int J Heat Mass Transfer 2013; 60:365–374.